

# Uncertainty Quantification-Driven Robust Design Assessment of a Swirler Geometry

Pamphile T. Roy<sup>a,\*</sup>, Guillaume Daviller<sup>a</sup>, Jean-Christophe Jouhaud<sup>a</sup>,  
Bénédicte Cuenot<sup>a</sup>

<sup>a</sup>*CFD Team, CERFACS, 42 Avenue Gaspard Coriolis, 31057 Toulouse cedex 1, France*

---

## Abstract

This paper presents an Uncertainty Quantification (UQ) study of a swirl injector geometry. Based on Large Eddy Simulations (LES) coupled with a mesh refinement strategy, the present work addresses a problem with a high dimensional parameter space consisting of 16 geometrical variables. Using real measurements, the Highest Density Region (HDR) method was used to reduce the parameter space to 6 random variables by uncovering correlations linked to the Additive Manufacturing (AM) process. Uncertainty Analysis (UA) reveals the sensitivity of the flow to the swirler geometry and shows in particular the robustness of the design to manufacturing tolerances. This work highlights the potential of UQ combined with LES for the robust design of industrial systems subjected to manufacturing deviations.

*Keywords:* Uncertainty Quantification, Uncertainty Analysis, Dimension reduction, Highest Density Regions, LES, Robust design

---

## 1. Introduction

At the heart of a turbomachine is the combustion chamber, fed with fuel by injectors. In order to stabilize the flame, swirled injectors are commonly used today [1]—see Fig. 1. By impelling a movement of rotation to the flow, a recirculation zone is created directly at the outlet of the injector. This ensures

---

\*Corresponding author  
Email address: [roy@cerfacs.fr](mailto:roy@cerfacs.fr) (Pamphile T. Roy )

sufficient residence time for the fuel to be consumed. The design of swirled injectors is of prime importance when seeking to reduce fuel consumption and pollutant emissions. Indeed, this is usually achieved via lean combustion which may lead to combustion instabilities and reduced extinction margins. When 10 considering environmental aspects, operability, efficiency, maintenance or even durability, the problem becomes a complex multiobjective optimization problem which remains a great challenge.

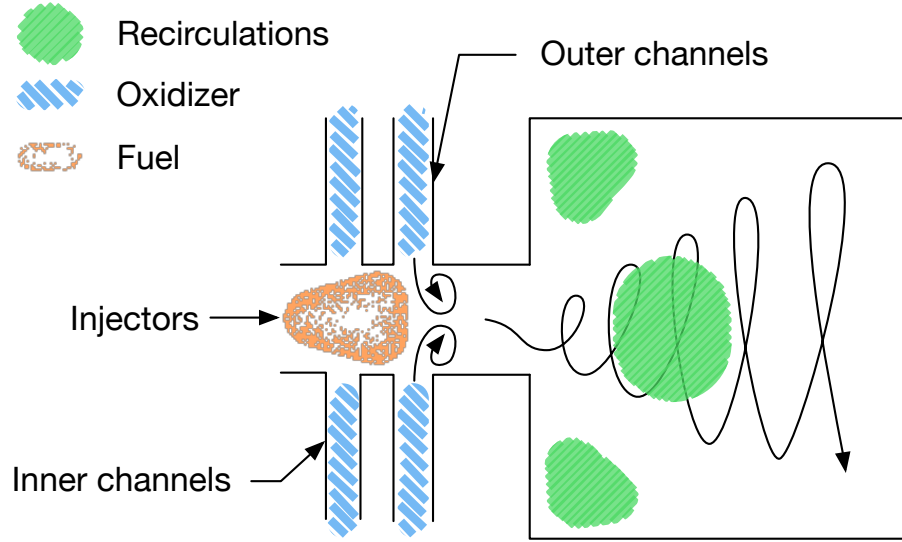


Figure 1: Sketch of a swirl burner consisting of two contra-rotative sets of oxidizer channels.

To help in the development of future engines, numerical simulations—and here Computational Fluid Dynamics (CFD) simulations—, have undoubtedly 15 become reliable and essential design tools [2, 3]. Recently, the use of Large Eddy Simulations (LES) coupled with a mesh adaptation strategy has demonstrated its capacity to identify the relevant physics of swirling flows [4]. From expert knowledge, the design of a swirl burner proceeds in three steps: (i) an exploratory phase is first performed using Reynolds-averaged Navier-Stokes (RANS) computations; (ii) the resulting possible geometries installed in the combustion 20 chamber are simulated using LES of turbulent combustion; (iii) prototypes are

manufactured and tests are performed. The first step allows to explore a large range of possibilities in terms of geometrical modifications (angles, number of channels, etc.) to meet requirements such as the swirl number, effective surface and permeability. The second step is performed to assess the combustion stability and the combustor performances in various operating conditions. Finally experiments are conducted to finalize the design.

For this last step, metal Additive Manufacturing (AM) [5, 6] is now in use. The AM technology has gained a lot of attention as it does not impose any constraint from the design point of view without sacrificing mechanical properties [7]. However, AM induces some uncertainties regarding the structural composition of the produced metallic systems, making this an active topic of research. In particular, geometrical uncertainties may result from the deposition method, the scanning method or even the powder size. Moreover, due to the complexity of some designs, it might not be possible to polish surfaces using standard mills. This may leave some defects which size depends on the quality of the whole process.

The present study aims to measure the effect of AM on the fluid motion. This is achieved through Uncertainty Quantification (UQ) [8] based on LES with varying geometry. A Principal Component Analysis (PCA) is first performed to build a reduced parameter space allowing to take into account all design variables. Then, uncertainties on the design variables are propagated in a series of 30 LES, providing summary statistics.

The paper is organized as follows: Section 2 presents the studied configuration as well as the LES numerical setup. Section 3 details the methodology used to reduce the parameter space. Results of the UQ study are then presented and analyzed in Section 4 and Section 5, respectively.

## 2. Configuration and Numerical Setup

### 2.1. The Swirled Injector

50      Figure 2 presents a sketch of the swirler studied in this work (also described in [4]) together with the computational domain. The swirler consists of two counter-rotating stages of 8 tangential vanes resulting in a rotational flow. A recirculation zone appears just downstream the swirler, which is paramount to combustion stability. In this study, no fuel is injected.

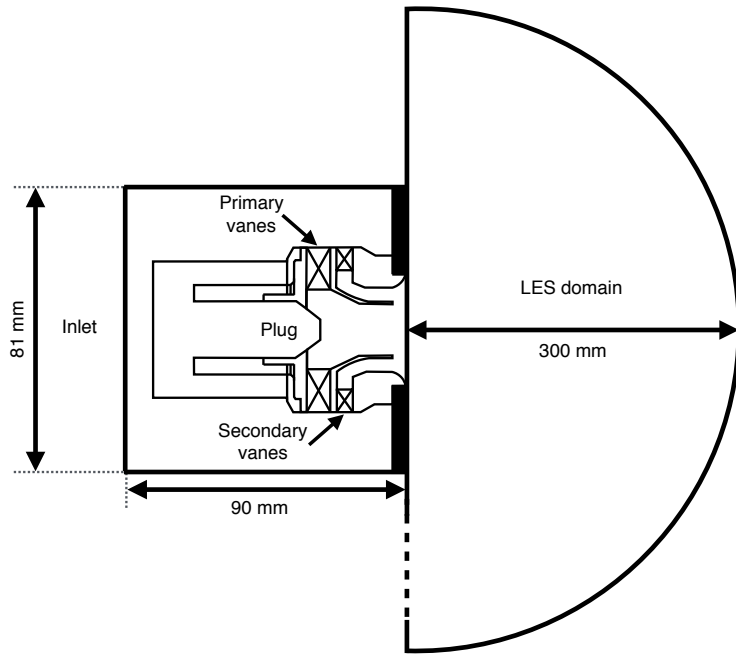


Figure 2: Schematic view of the configuration and the LES computational domain.

### 55      2.2. Numerical Setup

All simulations were performed using the compressible Navier-Stokes solver AVBP [9]. The finite-element scheme TTGC [10] was used on a tetrahedral mesh and LES equations were closed using the  $\sigma$ -model [11]. At the inlet and outlet boundaries Navier-Stokes Characteristic Boundary Conditions (NSCBC) 60 were applied [12], imposing the mass flow rates and the pressure, respectively.

All wall boundary conditions were specified as wall no-slip conditions without wall law models.

### 2.2.1. Mesh Adaptation Strategy

Due to the relative complexity of the geometry and the resulting mesh size,  
65 an Adaptive Mesh Refinement (AMR) strategy was used to reduce the CPU cost while preserving the quality of the solution, evaluated with the global pressure loss  $\Delta P$ . The AMR strategy used in this study is based on the methodology proposed in [4]: from the result obtained on an initial arbitrary mesh, a metric based on the time-averaged viscous dissipation field  $\overline{\Phi}$  is computed as:

$$\overline{\Phi} = \overline{(\mu + \mu_t) \left( \frac{\partial u_i}{\partial x_j} + \frac{\partial u_j}{\partial x_i} \right)^2}, \quad (1)$$

70 where  $\mu$  is the molecular viscosity and  $\mu_t$  the turbulent viscosity.

Then the mesh of the computational domain is adapted using the MMG3D library [13](noted *AD1*). This procedure is repeated with a second adaptation (noted *AD2*), so that the experimental pressure loss  $\Delta P$  is recovered (see Fig. 3). The computational details of one adaptation run are summarized in Table 1. In  
75 the end, with two mesh adaptation steps, one run required 25 000 CPU hours to simulate 40 ms of physical time.

Table 1: Summary of mesh adaptation for one simulation. Physical simulation time is constant at 40 ms.

	Coarse	AD1	AD2
number of cells ( $\times 10^6$ )	1.6	4.1	12.8
time step ( $\times 10^{-7}$ s)	0.59	0.47	0.20
CPU hours	5h30	2h20	9h30
number of cores	560	2800	2800
$\Delta P$ relative error	57,8 %	6,5 %	4,8 %

As shown in [4], this method converges and finally recovers the physics with a limited error on the pressure loss ( $\sim 5\%$ ). This is obtained thanks to the

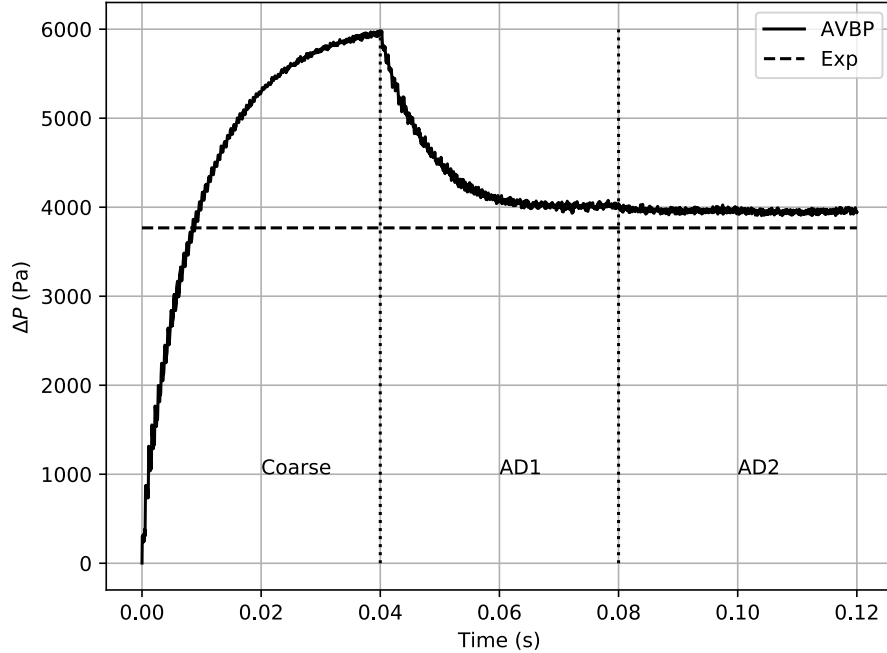


Figure 3: Evolution of the pressure loss computed with LES on the three different meshes successively with increasing resolution: *Coarse*, *AD1* and *AD2*. The dash line represents the experimental value of  $\Delta P$ .

choice of the viscous dissipation—which controls the irreversible losses—as the  
80 refinement metric. From Fig. 4 showing the evolution of the mesh, it appears that the mesh has mostly been refined around the plug tip and at the swirler exit. These zones indeed correspond to the zones where the dissipation is highest as seen in Fig. 5. This result also indicates that any geometrical deviation in these zones may result in a modified pressure loss.

#### 85 2.2.2. Simulation Strategy for UQ

In order to quantify the uncertainty on the flow physics, a sample of 30 LES was considered. The procedure used to generate this sample is detailed in Section 3. For each simulation, a new geometry has been constructed with up to 2% of variation in all channel dimensions—using the method presented in Section 3. Then, the mesh was automatically adapted using the aforementioned  
90

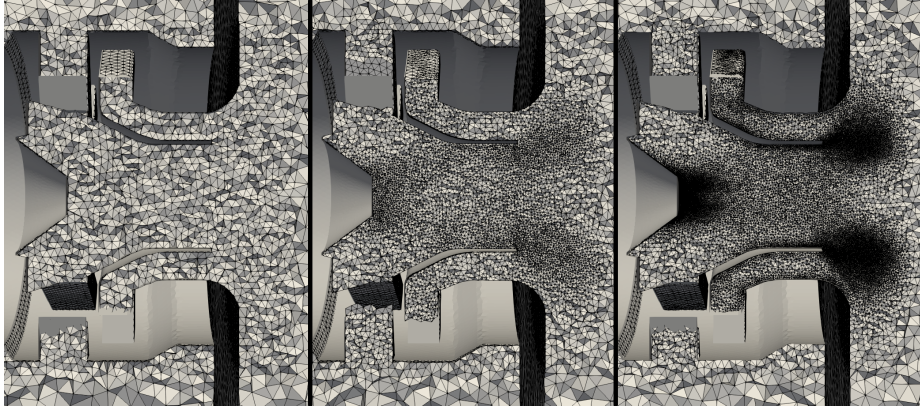


Figure 4: From left to right: coarse mesh, first adaptation  $AD1$  and second adaptation  $AD2$ .

methodology. This procedure ensures that the meshes are optimum for each configuration, with respect to the pressure loss. For the uncertainty analysis, results were averaged over 40 ms. The total computational cost for this UQ using LES is about 1 000 000 CPU hours. Thanks to high performance computing resources, the return time was only 2 days, which is satisfactory in the context of an industrial design process.

The *BATMAN* (Bayesian Analysis Tool for Modelling and uncertainty quantification) tool [14] was used to handle all simulations and perform the analysis. This open source python framework (<https://gitlab.com/cerfacs/batman>) is able to work with any code seamlessly as a *black-box*. It provides an easy workflow that constructs the design of experiments, launches each simulation and performs the statistical analysis and corresponding visualizations. It is built on top of the open source python library OpenTURNS [15]. *BATMAN* has been validated in multiple previous studies dealing with complex numerical solvers [16, 17].

### 2.3. Geometrical Uncertainties of the Swirler

Discrepancies in the size of the channels generated by AM have been measured. Figures 5 and 6 illustrate how a change of  $\sim 2\%$  in all channel dimensions—due to manufacturing dispersion—impacts the flow and the pressure loss  $\Delta P$ .

110 The two cases correspond to the maximum (case a) and minimum (case b)  
 impact on the pressure loss. These results were obtained from LES and the  
 numerical setup described in Section 2.2. Figure 5 shows the difference in total  
 dissipation field  $\bar{\Phi}$ , which explains the difference in pressure drop. Compared to  
 the pressure drop in the reference geometry, the two cases show a difference of  
 115 7.83% and 9.95% respectively for Fig. 5(a) and Fig. 5(b). A closer look allows  
 to identify the main region of difference at the tip of the plug, directly related  
 to the flow difference in the first stage of the swirler, as seen in Fig. 6. Indeed,  
 a small recirculation zone (at the tip of the plug) appears in the left case (a),  
 which almost disappears in the right case (b).

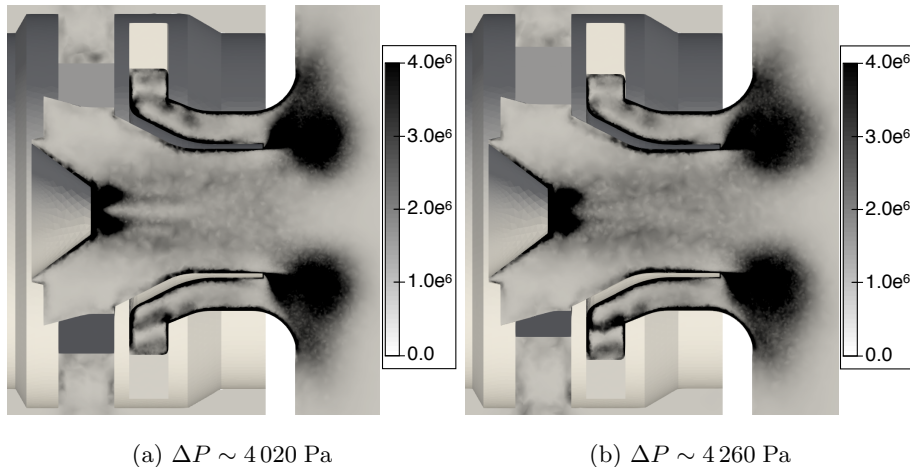


Figure 5: Fields of mean kinetic energy dissipation ( $\text{W}/\text{m}^3$ ) for two geometries with  $\sim 2\%$  channel size difference with the reference case.

120 **3. Dimensionality Reduction and Statistical Analysis of Uncertain  
 Parameters**

Performing a statistical analysis requires a large number of numerical simulations in order to converge statistical moments. If the number of parameters is also large, an even larger number of samples is required. In the present case (Section 2), the uncertain parameters are the dimensions of all 16 channels. For

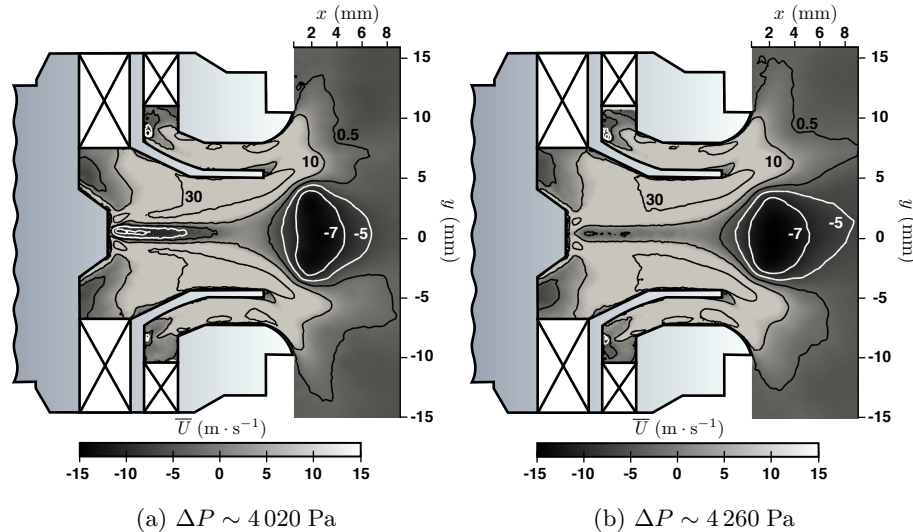


Figure 6: Field of mean axial velocity for two geometries with  $\sim 2\%$  channel size difference with the reference case. *Black* isocontours denote positive velocity, while *white* isocontours denote negative velocity.

each channel, this parameter induces a modification of the cross section area. However the channel dimensions, resulting from AM, are not independent and the number of independent parameters can be reduced. Indeed, AM is a layer-by-layer process which precision relies on the ability of the machine to build up and polish these layers. All channels of one stage being built simultaneously, a systematic bias is introduced.

A set of 5 various real swirl geometries issued from AM was obtained from an engine manufacturer. Thanks to the layering process, two groups of channels are considered to separate the two stages: (*i*) the inner set (first stage) of channels is noted  $s = in$ , and (*ii*) the outer set (second stage) of channels is noted  $s = ou$ . Data of each of these two groups is aggregated in the form of a function:  $d_s(i)$  with  $d$  the channel dimension,  $i$  the channel number and the subscript  $s$  standing for the inner or the outer set.

The dataset is then represented as a matrix, each line containing the curve  
 140  $d_s(i)$  corresponding to each channel geometry. In order to reveal the correlations

in the data and reduce the number of parameters for the UQ study, this matrix is decomposed using a Principal Component Analysis (PCA) [18], which allows to represent data with a finite number of modes. This compression process turns the functional representation into a scalar representation in a reduced space. The retained variance from the initial data increases with the number of modes of the PCA. In this work, more than 90% of the original dataset variance is retained with only three PCA components per stage, as shown in Fig. 7. The 16 independent uncertain parameters are then reduced to 6 independent parameters (three for each stage), while still accounting for 90% of the total variance of the original dataset.

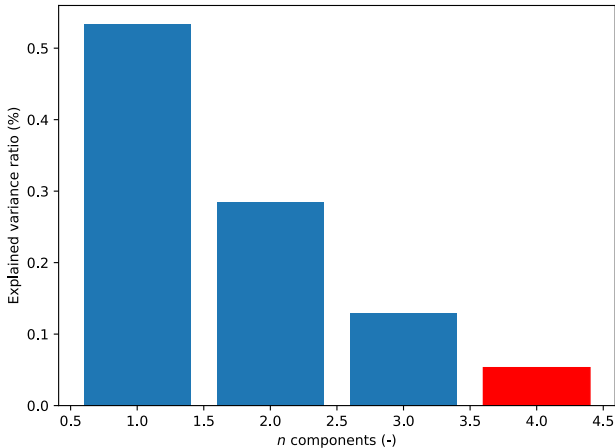


Figure 7: Contribution to the explained variance of the first four modes for the outer channels (similar results for inner channels are not shown). Summing the first three modes only (in blue) and ignoring the fourth mode (in red) corresponds to more than 90 % of the variance of the original dataset.

Within the reduced space of PCA components noted  $\mathbf{x}_r$ , the Highest Density Region (HDR) boxplot method [19] is used to summarize the data statistics and infer new swirler geometries. To determine the HDR, the Probability Density Function (PDF)  $f(\mathbf{x}_r)$  is built with a multivariate Kernel Density Estimation

(KDE) technique [20]. The PDF estimator  $\hat{f}(\mathbf{x}_r)$  is given by:

$$\hat{f}(\mathbf{x}_r) = \frac{1}{N_s} \sum_{i=1}^{N_s} K_{h_i}(\mathbf{x}_r - \mathbf{x}_{ri}), \quad (2)$$

where  $N_s$  is the number of samples and  $K_{h_i}(.) = K(./h_i)/h_i$  is the scaled kernel chosen for the modal probability density function with  $h_i$  the bandwidth for the  $i$ th component. In the present work  $K$  is the Gaussian kernel and  $h_i$  are optimized by cross-validation of the log-likelihood of the data. From this PDF estimator, the HDR reads:

$$R_\alpha = \left\{ \mathbf{x}_r : \hat{f}(\mathbf{x}_r) \geq f_\alpha \right\} \quad (3)$$

with  $f_\alpha$  such that  $\int_{R_\alpha} \hat{f}(\mathbf{x}_r) dx_r = 1 - \alpha$ . With this definition, the HDR corresponds to the region of highest PDF with a cumulative probability of  $1 - \alpha$ . The 50% and 90% HDR are computed, corresponding respectively to  $\alpha = 0.5$  and  $\alpha = 0.1$ . By construction a HDR develops around the maximum PDF  $\max\{\hat{f}(\mathbf{x}_r)\}$  which identifies the most probable mode. Transposed using the inverse transform from the reduced space to the original space, this most probable mode corresponds to the "central curve"—also referred to as the median curve. To summarize, in the original space the median curve corresponds to the most probable set of values that defines a swirler geometry manufactured with AM,  
155 while the 50% and 90% HDR express the data dispersion.  
160

The PDF estimator and the HDR allow to infer new realizations that are statistically relevant to the original dataset and can be used for the UQ analysis. This is done in the next section.

#### 4. Generation of datasets

165 In the 3 PCA-components space defined from the experimental database, a set of 30 points was sampled from a low discrepancy sequence of *Sobol'* (scrambled) [21, 22] which ensures a good coverage of low-dimensional parameter spaces. The 30 points are plotted in Figure 8 in 2D cuts of the 3D parameter space of each swirler stage. The PDF estimators obtained for each PCA  
170 component are shown in the plots placed along the diagonal of the figure.

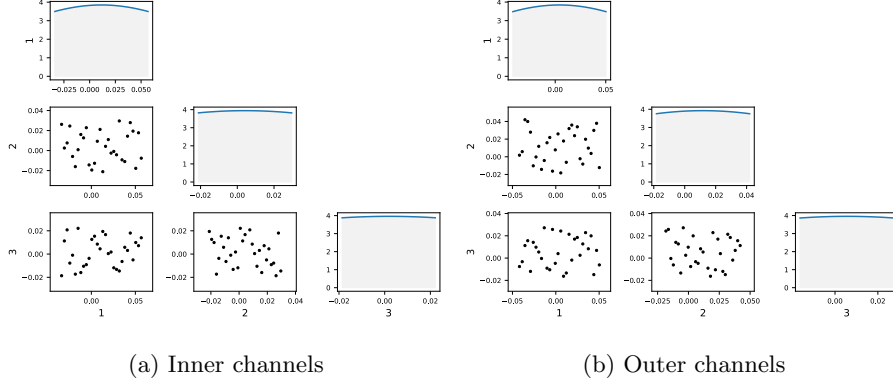


Figure 8: Bivariate principal component score plots of the 30 generated samples in the reduced PCA parameter spaces of the inner and outer stages. Each point corresponds to a curve sample. Probability distributions for each component are shown in the diagonal plots: *lines* represent the kernel PDF estimator and *Shaded* areas are histograms (from which are based the scaling of the *y-axis*).

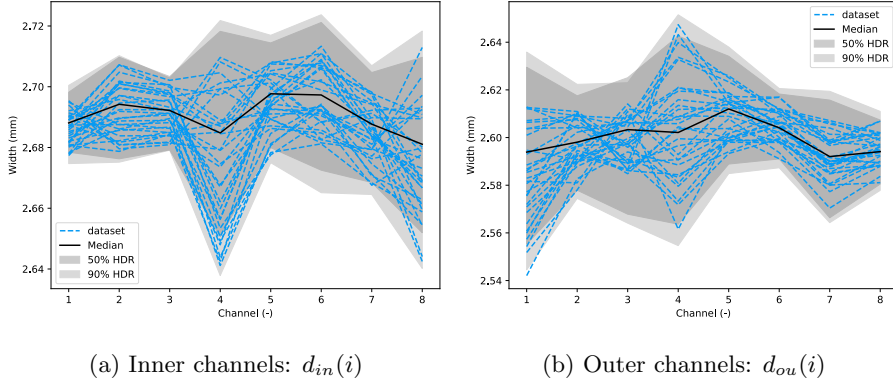


Figure 9: Statistics of channel dimensions: median curve (***bold solid*** line) and 50% and 90% HDR (***shaded*** areas). Blue ***dashed*** lines represent the 30 generated samples.

Figure 9 shows the 30 curves in the initial parameter space (channel dimensions) corresponding to the inverse transform of the 30 generated datasets. It can be noted that 30 curves are well distributed around the median line, inside the 90% HDR, confirming that the sampling is statistically relevant to the original dataset. Thus this method is able to reproduce statistically relevant scenarios of swirler geometries.  
175

The number of samples was chosen to minimize the computational time (see Section 2). From [23], it should be at least  $10n_{dim}$ , with  $n_{dim}$  the number of parameters, leading in our case to 60 samples. However, as we are interested in small variations in the parameter space, the variation of the quantity of interest (pressure loss) is not expected to exhibit strong linearities and it can be said that 30 simulations seems reasonable to describe it.

A larger initial database could reveal even more correlations between the parameters, allowing to further reduce the number of parameters. With the 5 datasets used here, a large dispersion of the different realizations is observed in Fig. 9. Still, it is clear that the 16 initial parameters of the 5 datasets are not independent, which is essential for the current study as keeping all 16 parameters independently would have required an enormous number of simulations.

## 5. Results and Discussion

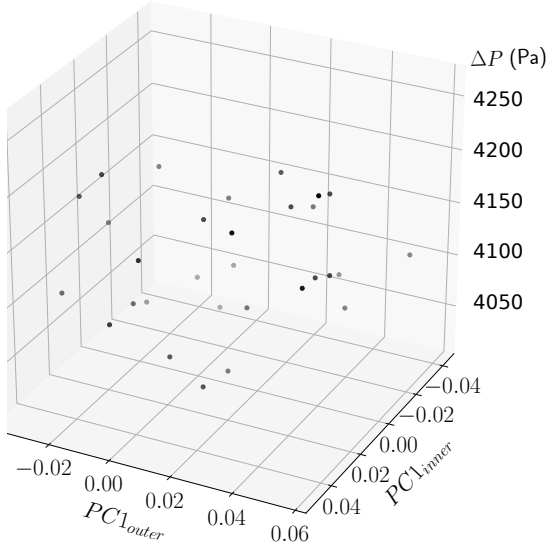


Figure 10: Pressure loss function of the first components of the reduced space.

Figure 10 shows the evolution of the pressure loss by varying the channel

dimensions. As the design of experiments consists of 6 parameters, the response is presented in a 2-dimensional plot where the first modes of both inner and outer channels are used. Indeed the first modes contribute the most to the variance of the data. In Fig. 10 no cluster of points appears at any particular level 195 of pressure drop and the pressure loss distribution is relatively uniform among the samples. Summary statistics are presented in Table 2 and the probability distribution of the ensemble is shown in Fig. 11. All these results indicate that the response of the system to these geometrical modifications is rather uniform: the geometrical uncertainties are transmitted through the system without 200 amplification.

Table 2: Summary statistics of the pressure drop of the 30 LES.

	Mean	Median	Std	Min	Max
Pressure drop (Pa)	4128	4133	65	4020	4260

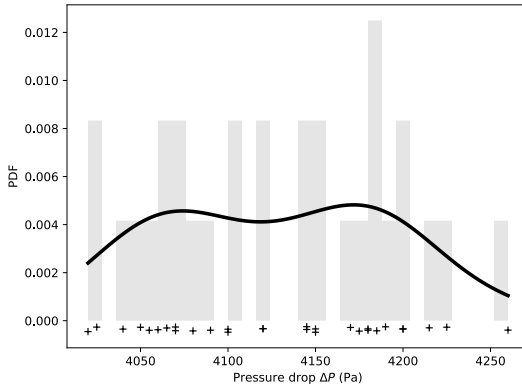


Figure 11: PDF of the pressure loss over the dataset (black line) reconstructed using KDE. Crosses represent the samples, and the shaded area is a histogram view.

As a consequence of this uniformity with no clear structure, it is difficult to build a reduced model. Several surrogate model strategies available in BATMAN—see Section 2—such as Gaussian process, polynomial chaos and Radial Basis Functions were tested, but none of these methods were able to

<sup>205</sup> fit the data and infer a satisfactory result. The reported quality—assessed by Leave-one-out cross validation [24]—was negative, which implies that the tested surrogate models are worse than a simple constant guess.

<sup>210</sup> To further analyse the results, Fig. 12 shows the variation of the pressure loss with the total channel section area for each simulation. Again no clear pattern is making out. The swirl numbers—definition from Merkle [25]—for cases with maximum, minimum and middle value of pressure drop are summarized in Table 3. It is interesting to see that despite pressure drop variation, the swirl number which drives the characteristics of the flow stays within negligible variation close to the theoretical value of  $S = 0.76$  in all three cases. These <sup>215</sup> observations are confirmed by the comparison of the mean axial velocity profiles downstream the nozzle exit compared with PIV measurement for the same three cases (Fig. 13). Details and discussion about PIV are given in Daviller *et al.* [4]. Very close curves are obtained for the three LES at the shown positions. This means that, in accordance with the unchanged swirl number, no significant <sup>220</sup> change occurs in the flow field downstream the nozzle.

Table 3: Swirl numbers for three different geometries.

	$\Delta P_{middle} = 4\,145 \text{ Pa}$	$\Delta P_{min} = 4\,020 \text{ Pa}$	$\Delta P_{max} = 4\,260 \text{ Pa}$
Swirl number	0.7609	0.7582	0.7639

<sup>225</sup> Although the construction of a surrogate model is not feasible in this case, the present uncertainty analysis highlights the intrinsic and chaotic variability of a self-compensation mechanism in the generated statistical data. This can be explained by: (*i*) the nature of the geometrical modifications, where some channels are widened while others are tightened, limiting the overall impact on the pressure loss; and (*ii*) the amplitude of these modifications which is very small compared to the width of the channels. Indeed, manufacturing defects were limited to a maximum 2% of the cross section area of a channel, consistently with real observation of AM. Note that in such situation, the ability of the solver

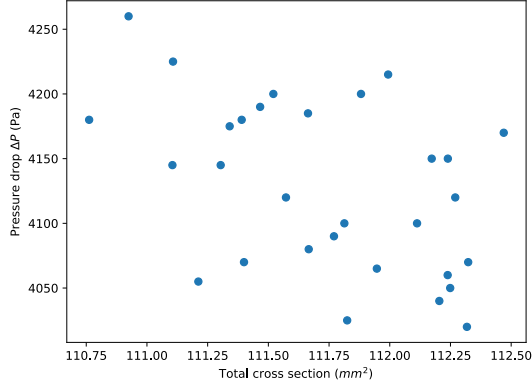


Figure 12: Pressure drop as a function of the total cross section channel area. Each point represents a sample.

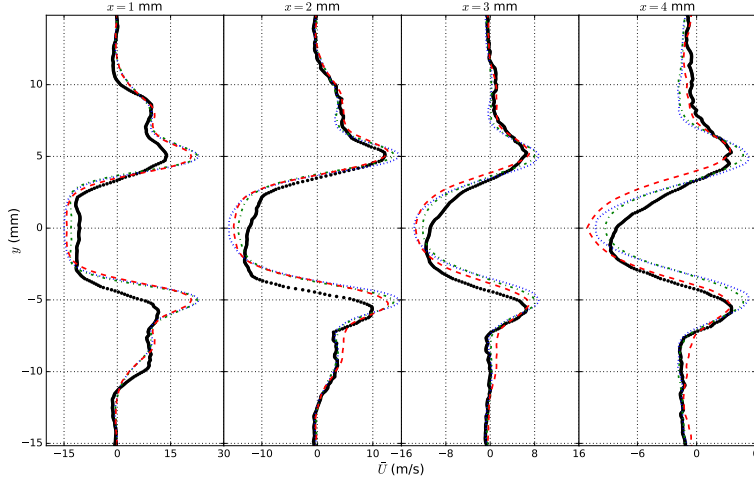


Figure 13: Mean axial velocity profiles at four axial locations (from left to right  $x = 1, 2, 3, 4$  mm) obtained with LES and in the experimental setup (black circles). Dotted lines  $\Delta P_{middle} = 4\,145$  Pa, dashed-dotted lines  $\Delta P_{min} = 4\,020$  Pa, dashed lines  $\Delta P_{max} = 4\,260$  Pa.

to respond with the correctly adapted physics is paramount. To check this, the relative numerical error on the pressure drop was estimated and found less than 1% which is sufficient to capture with accuracy the pressure drop induced variation by geometrical modification of the order of  $\simeq 5\%$ . Thus, the solver

accuracy is sufficient and the results are considered reliable.

<sup>235</sup> **6. Conclusions**

The purpose of this work was to perform an Uncertainty Quantification (UQ) study of a swirler geometry. More precisely, this study focused on geometry deviations due to Additive Manufacturing (AM) and their effects on the pressure loss. As the number of parameters required to characterize the configuration was <sup>240</sup> high, a Principal Component Analysis (PCA) was used, allowing to cut down the number of parameters from 16 to 6 independent variables. Statistic analysis based on Highest Density Region (HDR) highlighted the non-independence of the geometrical parameters and thus the impact of AM. Thanks to a mesh adaptation strategy, a set of 30 different statistically representative cases was <sup>245</sup> accurately simulated with Large Eddy Simulations (LES). The uncertainty analysis then led to an overall view of the variation of the pressure drop induced by geometry changes. Results show that slight discrepancies in the swirler channel dimensions lead to slight differences in the pressure loss, without amplification or damping. This conclusion also holds for the flow, as shown by the comparison of the swirl numbers and velocity profiles. This is a critical information for <sup>250</sup> engine manufacturers, as it means that AM will not affect the flow exiting the swirler and the stability of the flame developing downstream.

The analysis of the intrinsic variability of the system did not exhibit any <sup>255</sup> noticeable pattern. As a consequence, no surrogate model could be built. This is explained by the nature of the modifications and most importantly by their amplitude. Augmenting the range of variability in the system, exploring for example other designs, would increase the impact on the pressure loss.

The UQ method used in this work, combining data reduction and high-fidelity LES, paves the way for systematic uncertainty studies in the design phase <sup>260</sup> of industrial systems to take into account manufacturing defects. This may lead to the determination of optimized manufacturing tolerances, and finally to significant cost saving.

## Acknowledgements

The authors acknowledge Patrick Duchaine from Safran Helicopter Engines  
265 for his insights on their technologies as well as Bertrand Iooss and Michael  
Baudin from MRI (EDF R&D) for helpful discussions on uncertainty quantification  
and support on OpenTURNS. The financial support provided by all the  
CERFACS shareholders (AIRBUS Group, Cnes, EDF, Météo-France, ONERA,  
SAFRAN and TOTAL) is greatly appreciated and we thank them for enabling  
270 the achievement of such research activities. This work was granted access to the  
HPC resources of [CCRT/CINES/IDRIS] under the allocation [x20162a6074]  
made by GENCI.

## References

- [1] d. g. lilley, swirl flows in combustion: a review, *aiaa journal* 15 (8) (1977)  
275 1063–1078. doi:[10.2514/3.60756](https://doi.org/10.2514/3.60756).
- [2] j. sacks, w. j. welch, t. j. mitchell, h. p. wynn, design and analysis of  
computer experiments, *statistical science* 4 (4) (1989) 409–423. doi:  
10.1214/ss/1177012413.
- [3] a. i. j. forrester, a. j. keane, recent advances in surrogate-based optimization,  
280 *progress in aerospace sciences* 45 (1-3) (2009) 50–79. doi:[10.1016/j.paerosci.2008.11.001](https://doi.org/10.1016/j.paerosci.2008.11.001).
- [4] g. daviller, m. brebion, p. xavier, g. staffelbach, j.-d. müller, t. pointsot, a  
mesh adaptation strategy to predict pressure losses in les of swirled flows,  
flow, turbulence and combustion doi:[10.1007/s10494-017-9808-z](https://doi.org/10.1007/s10494-017-9808-z).
- 285 [5] w. e. frazier, metal additive manufacturing: a review, *journal of materials engineering and performance* 23 (6) (2014) 1917–1928. doi:[10.1007/s11665-014-0958-z](https://doi.org/10.1007/s11665-014-0958-z).

- [6] w. j. sames, f. a. list, s. pannala, r. r. dehoff, s. s. babu, the metallurgy and processing science of metal additive manufacturing, *international materials reviews* 61 (5) (2016) 315–360. doi:10.1080/09506608.2015.1116649.
- [7] j. j. lewandowski, m. seifi, metal additive manufacturing: a review of mechanical properties, *annual review of materials research* 46 (1) (2016) 151–186. doi:10.1146/annurev-matsci-070115-032024.
- [8] b. iooss, a. saltelli, introduction to sensitivity analysis, in: *handbook of uncertainty quantification*, Springer International Publishing, Cham, 2015, pp. 1–20.
- [9] t. schønfeld, m. rudgyard, steady and unsteady flow simulations using the hybrid flow solver avbp, *aiaa j.* 37 (11) (1999) 1378–1385.
- [10] o. colin, m. rudgyard, development of high-order taylor-galerkin schemes for unsteady calculation, *j. comp. physics* 162 (2) (2000) 338–371.
- [11] f. nicoud, h. baya toda, o. cabrit, s. bose, j. lee, using singular values to build a subgrid-scale model for large eddy simulations, *phys. fluids* 23.
- [12] t. poinsot, s. k. lele, boundary conditions for direct simulations of compressible viscous flows, *j. comp. physics* 101 (1) (1992) 104–129.
- [13] c. dapogny, c. dobrzynski, p. frey, three-dimensional adaptive domain remeshing, implicit domain meshing, and applications to free and moving boundary problems, *j. comp. physics* 262 (2014) 358–378.
- [14] p. t. roy, s. ricci, r. dupuis, r. campet, j.-c. jouhaud, c. fournier, batman: statistical analysis for expensive computer codes made easy, *the journal of open source software* 3 (21) (2018) 493. doi:10.21105/joss.00493.
- [15] m. baudin, a. dutfoy, b. iooss, a.-l. popelin, openturns: an industrial software for uncertainty quantification in simulationarXiv:1501.05242.
- [16] p. t. roy, n. el moçayd, s. ricci, j.-c. jouhaud, n. goutal, m. de lozzo, m. c. rochoux, comparison of polynomial chaos and gaussian process surrogates

- 315 for uncertainty quantification and correlation estimation of spatially distributed open-channel steady flows, stochastic environmental research and risk assessment (2017) 1–29doi:10.1007/s00477-017-1470-4.
- [17] p. t. roy, l. m. segui, j.-c. jouhaud, l. gicquel, resampling strategies to improve surrogate model-based uncertainty quantification: application to les 320 of ls89, international journal for numerical methods in fluids (march) (2018) 1–21. doi:10.1002/fld.4504.
- [18] anindya chatterjee, an introduction to the proper orthogonal decomposition, current science 78 (7).
- [19] r. j. hyndman, h. l. shang, rainbow plots , bagplots and boxplots for functional data, journal of computational and graphical statistics 19 (2009) 325 29–45.
- [20] m. p. wand, m. c. jones, kernel smoothing, springer us, boston, ma, 1995. doi:10.1007/978-1-4899-4493-1.
- [21] m. cavazzuti, design of experiments, in: optimization methods: from theory to design, springer berlin heidelberg, 2013, pp. 13–42. doi:10.1007/330 978-3-642-31187-1\_2.
- [22] s. kucherenko, d. albrecht, a. saltelli, exploring multi-dimensional spaces: a comparison of latin hypercube and quasi monte carlo sampling techniques, the 8th imacs seminar on monte carlo methods (2015) 1–32doi:10.1016/j.ress.2017.04.003. 335
- [23] a. i. forrester, a. sóbester, a. j. keane, multi-fidelity optimization via surrogate modelling, proceedings of the royal society a: mathematical, physical and engineering sciences 463 (2008) (2007) 3251–3269. doi:10.1098/rspa.2007.1900.
- [24] r. kohavi, a study of cross-validation and bootstrap for accuracy estimaiton 340 and model selection, in: international joint conference on artificial intelligence, 1995.

- [25] k. merkle, einfluss gleich- und gegensinniger drehrichtung der ver-  
brennungsluftströme auf die stabilisierung turbulenter doppeldrall-  
<sup>345</sup> diffusionsflammen, Ph.D. thesis, universität fridericiana karlsruhe (2006).